J. Fluid Mech. (2011), *vol.* 666, *pp.* 391–413.
doi:10.1017/S002211201000488X

Leakage from gravity currents in a porous medium. Part 1. A localized sink

JEROME A. NEUFELD†, DOMINIC VELLA, HERBERT E. HUPPERT AND JOHN R. LISTER

Institute of Theoretical Geophysics, Department of Applied Mathematics and Theoretical Physics, University of Cambridge, CMS, Wilberforce Road, Cambridge CB3 0WA, UK

(Received 3 March 2010; revised 3 August 2010; accepted 17 September 2010)

We consider the buoyancy-driven flow of a fluid injected into a semi-infinite porous medium bounded by a horizontal impermeable barrier through which a single localized sink allows leakage of the injected fluid. Our study is motivated by the geological sequestration of carbon dioxide (CO_2), which is less dense than the ambient water, and the possibility that fissures in the bounding 'cap' rock may therefore compromise the long-term storage of CO_2. A theoretical model is presented in which the leakage through the sink, or fissure, is driven by the hydrostatic pressure at the sink of the injected buoyant fluid. We determine numerical solutions for the evolution of the gravity current in the porous medium and for the quantity of fluid that escapes through the sink as a function of time. A quantity of considerable interest is the efficiency of storage, which we define as the flux of fluid that is stably stored relative to the amount injected. At the later stages in the evolution of the current, the region near the source and sink reaches a quasi-steady state. We find analytical solutions to this asymptotic state which show that the efficiency of storage decreases to zero like $1/\ln t$, where t is the time since initiation of the current, and predict a dependence on the properties of the sink in agreement with our numerical results. The implications of this result for the geological sequestration of CO_2 are discussed.

Key words: gravity currents, porous media

1. Introduction

The buoyancy-driven flow of fluids within porous media is a rich research field with an enormous range of applications in the natural and industrial worlds. Important examples include the flow of groundwater in aquifers, the migration of pollutants, the motion of oil and natural gas in petroleum reservoirs and the characterization of geothermal systems (see, for example, Bear 1972; Phillips 2009). More recently, interest has been focused on the injection of carbon dioxide (CO_2) into the Earth's subsurface as a means of mitigating emissions of this greenhouse gas due to human activity (Orr 2009). The proposed technology consists of capturing CO_2 from stationary sources such as power stations, compressing the gas, and injecting it into unused aquifers or old oil and gas reservoirs. The CO_2 is injected as a supercritical fluid which is less dense than the ambient fluid and therefore rises to the top of the reservoir until it encounters a relatively impermeable cap rock. Its vertical motion impeded,

† Email address for correspondence: j.neufeld@damtp.cam.ac.uk

the CO_2 then spreads beneath the mainly horizontal cap rock driven by the density contrast between the two fluids. Such buoyancy-driven motion has spurred many recent studies of migration within the subsurface (Huppert & Woods 1995; Lyle *et al.* 2005; Nordbotten & Celia 2006; Vella & Huppert 2006; Bickle *et al.* 2007; Hesse *et al.* 2007; Farcas & Woods 2009; Neufeld & Huppert 2009; Woods & Farcas 2009). Spreading currents of buoyant CO_2 will sample a large areal extent of the bounding cap rock, giving rise to concerns that they may encounter localized high-permeability regions in the cap rock ultimately leading to leakage of CO_2 back into the atmosphere. The possibility of leakage motivates our study into the effect of leakage pathways on the volume and propagation of buoyant currents in porous media.

Buoyancy-driven flows or gravity currents within a uniform and unconfined porous medium have been studied by Barenblatt (1996), Anderson, McLaughlin & Miller (2003) and Lyle *et al.* (2005). These studies, and others reviewed by Huppert (2006), have shown that porous gravity currents quickly reach a state in which their horizontal extent greatly exceeds their vertical scale so that the pressure is approximately hydrostatic. Flow in horizontal strata is thus driven by gradients in the depth of the current, which leads to the flow being described by a single nonlinear evolution equation for the depth. In the absence of any fault or fracture, this evolution equation admits a similarity solution from which the spreading of such subsurface flows can be quickly and effectively evaluated (Lyle *et al.* 2005; Bickle *et al.* 2007).

Motivated by flows through heterogeneous formations, models of porous gravity currents have been extended to include both diffuse and discrete leakage. Diffuse leakage through a bounding surface of reduced, but non-zero, permeability has been examined by Pritchard, Woods & Hogg (2001), who considered the limiting case of a thin low-permeability layer. This work was subsequently extended to examine two-dimensional drainage through a deep low-permeability layer (Pritchard & Hogg 2002) motivated by related studies on the flow of viscous fluids over a deep porous medium (Acton, Huppert & Worster 2001). The effect of leakage through thin low-permeability layers has also been investigated theoretically by Neufeld & Huppert (2009) spurred by seismic images of a CO_2 plume spreading at the Sleipner injection site in the North Sea (Bickle *et al.* 2007). Experimental work on drainage from axisymmetric currents into deep porous media has been performed by Spannuth *et al.* (2009), and confirmed the theoretical models of drainage over a deep porous medium. More recently, the effect of capillary forces between the injected and ambient fluids has been incorporated into models characterizing diffuse leakage between layers (Farcas & Woods 2009; Woods & Farcas 2009).

While there has been substantial research on drainage through uniform layers of differing permeability, models of drainage through discrete fractures, fissures or abandoned well-heads are in their infancy. Early work by Pritchard (2007) examined two-dimensional flow in which there is leakage from active faults spaced symmetrically on either side of a line of injection. Subsequent work by Neufeld, Vella & Huppert (2009) examined the dynamics of leakage from a single line sink placed some distance from the line of injection. Their study focused attention on the fraction of fluid that is sequestered beneath the cap rock and not leaked. They also confirmed the validity of these theoretical models using analogue laboratory experiments. In contrast to these two works on leakage from gravity currents, Avci (1994), Nordbotten, Celia & Bachu (2004) and Nordbotten *et al.* (2005) examined leakage from compressible currents in confined aquifers. These models incorporated the compressibility of both the porous medium and the injected fluid, but did not consider buoyancy-driven flow governed by gradients in the height of the current.

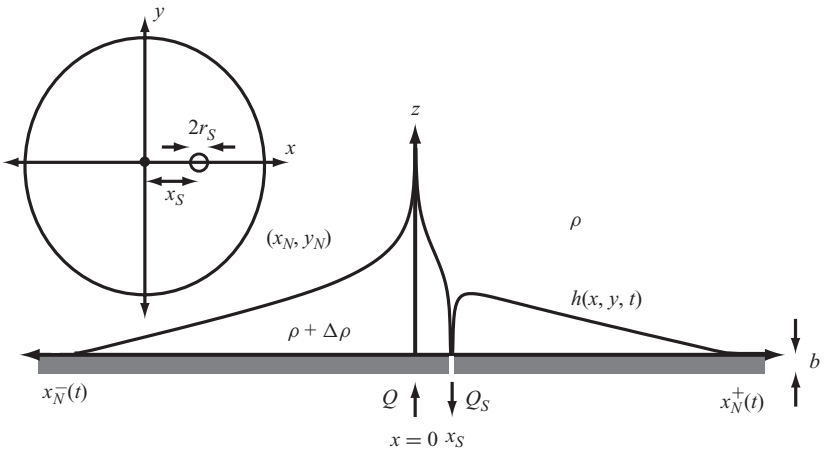

FIGURE 1. Illustration of the spreading of a dense current within a porous medium in which a sink at $(x, y) = (x_S, 0)$ allows fluid to leak from the system. The left inset shows a planview of the spreading current along with the position of the source and sink. The profile in the main figure shows a cross-section through a typical current taken along the line $y = 0$.

The present work extends the approach of Pritchard (2007) and Neufeld *et al.* (2009) to examine the spread of a buoyant gravity current from a point source in a porous medium with a horizontal boundary through which a cylindrical sink, of finite radius, allows leakage through the bounding cap rock. In § 2, we begin by introducing the geometry of the reservoir, the equations describing the propagation of the gravity current and those describing leakage through the sink. The consequent evolution is first evaluated numerically, from which we obtain the long-term efficiency of storage in § 3. The behaviour of the numerical solutions in the long-time limit motivates an asymptotic analysis of both the structure of the current and its effect on leakage, which we present in § 4. We discuss the application of our analysis to the geological sequestration of CO_2 in § 5 and present some concluding remarks in § 6.

2. Formulation

2.1. *Geometry*

We consider the spread of a fluid of density $\rho + \Delta\rho$ injected at a constant volume flux q into a semi-infinite porous medium of permeability k, saturated with fluid of density ρ, as illustrated in figure 1. Fluid is injected at the origin and the resultant flow is bounded below by a horizontal impermeable seal at $z = 0$ of thickness b along which the current spreads. The behaviour of such density-driven flows is identical when dense fluid is injected at the base of a porous medium (as shown in figure 1) or when light fluid is injected at the top of an aquifer beneath an impermeable seal, as would be the case in a typical scenario for geological sequestration of CO_2; for clarity, we describe the case of a dense fluid above an impermeable seal, but emphasize that all our results would apply equally to the case of a buoyant fluid below an impermeable seal. Leakage through the impermeable seal occurs only in a localized region centred on $(x, y) = (x_S, 0)$, where a cylindrical sink of radius r_S and permeability k_S allows for leakage from the reservoir. A sink of this geometry might model, for example, an abandoned well that penetrates the cap rock.

Since the porous medium is assumed semi-infinite, the pressure gradients associated with displacement of the ambient fluid are much less than those in the gravity current, and flow in the ambient fluid plays no dynamic role. A similar argument would apply to a finite-depth porous layer provided the depth of the gravity current is much less than that of the layer.

For simplicity, we assume that the interface between the injected and ambient liquid is sharp and can be described by $z = h(x, y, t)$, where h is the depth of the current. Thus, we neglect the effects of dispersion, of any interfacial energy between the injected and ambient fluids, and of any differences in viscosity, which can all act to create a transition zone of mixed phase (e.g. Bolster, Dentz & Carrera 2009). This assumption is unlikely to be strictly valid either for the injection of CO_2 into saline aquifers or for the injection of water or CO_2 into oil reservoirs, which will likely lead to multiphase currents whose saturation (of CO_2) varies with depth. Variations in saturation are reduced in density-dominated flows such as those considered here (see Lake 1989, for example). Hence, we still expect the methodology outlined below to capture the form of leakage when the flow is driven principally by the density contrast between injected and ambient fluids. Moreover, we anticipate that though multiphase effects will affect some of the quantitative details of the flow, they will not significantly affect the qualitative form of the current, and the additional complexity of the model would obscure the analysis and the interesting effects of geometry.

2.2. *Leakage and propagation*

We assume that the pressure drops from the hydrostatic overpressure $\Delta\rho g h$ at the mouth of the sink to the ambient reservoir pressure over a vertical distance b, which we imagine would typically be the thickness of the cap rock. Therefore, following the approach of Pritchard (2007) and Neufeld *et al.* (2009), the rate of leakage is proportional to the excess weight of the fluid above the sink region. The vertical Darcy velocity within the sink is therefore given by

$$v_s(x, y, t) = -\frac{k_S}{\mu}\frac{\Delta\rho g h}{b}, \quad |\zeta - \zeta_S| < r_S, \tag{2.1}$$

where k_S is the permeability of the sink, g is the acceleration due to gravity and $\zeta = x + \mathrm{i}y$ is a representation of the point (x, y) in the complex plane. (In this representation the centre of the sink is given by $\zeta_S \equiv x_S$.) For simplicity, we neglect the weight of the fluid within the sink itself and note that this additional effect can be incorporated in a relatively straightforward manner (Neufeld *et al.* 2009). In particular, incorporating the weight of fluid within the sink would lead to a somewhat greater effective sink strength.

Within the remainder of the current, flow is predominantly horizontal and therefore the pressure is effectively hydrostatic. We note that when the thickness of the porous medium or reservoir greatly exceeds that of the current, the spread of the current is driven principally by the density contrast, $\Delta\rho$, between injected and ambient fluids, except in the immediate vicinity of the injection and leakage points (see Lyle *et al.* 2005). The horizontal gradients of the hydrostatic pressure $\Delta\rho g h$ drive a flow with Darcy velocity $k\Delta\rho g\nabla h/\mu$ in the current over a height h. Applying mass conservation and noting that the interface moves with the pore velocity, we find that

$$\frac{\partial h}{\partial t} - \gamma\nabla\cdot(h\nabla h) = -\gamma\frac{k_S}{k}\frac{h}{b}\mathscr{F}(\zeta;\zeta_S, r_S) \tag{2.2}$$

(Lyle *et al.* 2005; Neufeld *et al.* 2009), where $\gamma = k\Delta\rho g/\phi\mu$ is the characteristic buoyancy velocity within the reservoir, the right-hand side of (2.2) represents leakage

through the sink, and

$$\mathscr{F}(\zeta\,;\zeta_S, r_S) \equiv \begin{cases} 0, & |\zeta - \zeta_S| > r_S, \\ 1, & |\zeta - \zeta_S| < r_S \end{cases} \tag{2.3}$$

describes a circular sink situated at $\zeta = \zeta_S$ with radius r_S. The evolution of the current described by (2.2) is subject to the boundary conditions

$$\lim_{r\to 0}\left[2\pi r\gamma h\frac{\partial h}{\partial r}\right] = -q, \quad [\boldsymbol{n}\cdot(\gamma h\nabla h)]_{\boldsymbol{r}_N} = 0, \tag{2.3a,b}$$

which describe respectively the constant flux q input at the origin and the requirement that there be no loss or gain of fluid at the nose of the current. Here $\boldsymbol{r}_N = (x_N, y_N)$ is the curve defining the footprint or outer edge of the current and $\boldsymbol{n}$ is the normal to this curve.

2.3. *Non-dimensional formulation*

The introduction of a sink at a distance x_S from the source introduces a natural length scale to the problem. Hence, we do not expect a similarity solution and instead non-dimensionalize the problem as follows. We scale all horizontal lengths with x_S, and the current thickness and the time by the scales

$$H \equiv (q/\gamma)^{1/2} \quad \text{and} \quad T \equiv \frac{x_S^2}{(q\gamma)^{1/2}}, \tag{2.4a,b}$$

respectively. Using dimensionless variables from now on, we write (2.2) as

$$\frac{\partial h}{\partial t} - \nabla\cdot(h\nabla h) = -\lambda h\mathscr{F}(\zeta\,;1,\epsilon), \tag{2.5}$$

where

$$\lambda \equiv \frac{k_S}{k}\frac{x_S^2}{b(q/\gamma)^{1/2}}. \tag{2.6}$$

is the dimensionless strength of the sink, and $\epsilon = r_S/x_S$ is its dimensionless radius. The boundary conditions are

$$\lim_{r\to 0}\left[2\pi rh\frac{\partial h}{\partial r}\right] = -1, \quad [\boldsymbol{n}\cdot(h\nabla h)]_{\boldsymbol{r}_N} = 0. \tag{2.7a,b}$$

The drainage law (2.1) can be averaged over the area of the sink to provide a measure of the total flux of fluid leaking from the system. By relating the total flux leaking from the system to the average height above the sink, we write the leakage flux as $\Lambda\bar{h}$, where

$$\Lambda \equiv \pi\epsilon^2\lambda \tag{2.8}$$

is an effective sink strength,

$$\bar{h} \equiv \frac{1}{\pi\epsilon^2}\int_0^{2\pi}\int_0^{\epsilon} h\tilde{r}\,\mathrm{d}\tilde{r}\,\mathrm{d}\theta \tag{2.9}$$

is the mean depth of the current above the sink, and $\tilde{r}$ is the local radial coordinate within the sink. The effective sink strength Λ is the radial analogue of the width-averaged sink strength used by Pritchard (2007) and Neufeld *et al.* (2009) and combines both the permeability and areal extent of the sink. When $\epsilon \ll 1$, the behaviour of the system is characterized by the single dimensionless parameter Λ, and

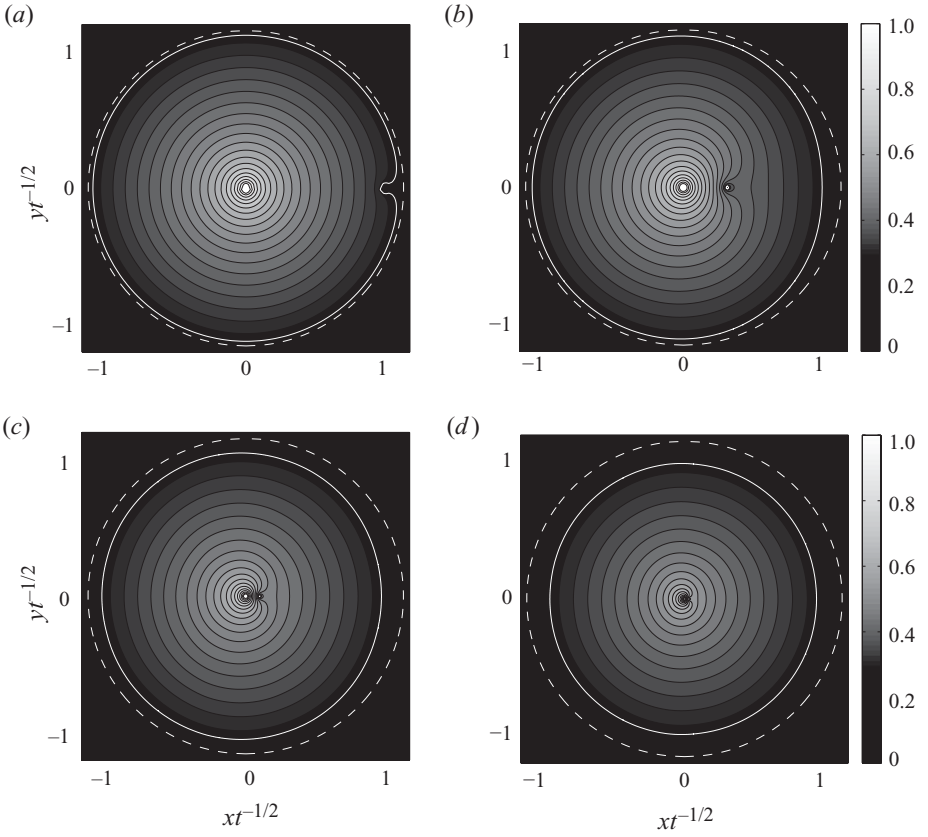

FIGURE 2. Contour plots of the height of the current at (*a*) $t=1$ (*b*), $t=10$ (*c*) $t=100$ and (*d*) $t=1000$ for $\Lambda=20$ and $\epsilon=0.036$. These correspond to (*a*) just after the end of the early self-similar stage, (*b*) an intermediate stage and (*c*, *d*) late stages in the current's evolution. Horizontal dimensions in each figure have been rescaled by $t^{-1/2}$ to highlight the increasing importance of leakage as time increases. To aid the eye, the edge of the current is demarcated by the solid white curve. The corresponding axisymmetric similarity solution, in the absence of leakage, is shown by the dashed white curve.

therefore in what follows we report our results in terms of Λ and direct the reader to Appendix B for a more detailed description of the local behaviour within the sink.

3. Numerical results for a spreading current

The evolution of a gravity current within a porous medium from which the fluid can escape through a finite-size sink as described by (2.5) and (2.7) was found numerically using an alternating-direction implicit scheme as outlined in Appendix A. Fluid was injected at the central grid cell and the spreading was calculated using a flux-conservative scheme assuming symmetry about the line $y=0$. The drainage law (2.1) was applied over 20 cells centred about $(x, y)=(1, 0)$, with grid resolution $\Delta x=\Delta y=1/101$ and an effective sink radius $\epsilon\approx 0.04$ (see Appendix A for details). The evolution, illustrated by the contour plots in figure 2, can be subdivided into three stages: an early, self-similar regime, an intermediate regime in which the sink has a leading-order effect on the planview of the current, and a long-time regime in which the current has spread well beyond the source–sink region.

At early times, $t < 0.75$, before the edge of the current reaches the sink where leakage takes place, the current spreads in a self-similar manner. Chen, Goldenfeld & Oono (1991) and Lyle *et al.* (2005) found that, for axisymmetric porous currents fed by a constant flux, the maximum radial extent is given by

$$r_N = \eta_N t^{1/2}, \tag{3.1}$$

where $\eta_N \simeq 1.155$. The vertical profile of the current can be described in terms of a similarity variable $\eta = rt^{-1/2}$ or a normalized similarity variable $\xi \equiv \eta/\eta_N$ by

$$h(r, t) = \eta_N^2 f(\xi), \tag{3.2}$$

where $f(\xi)$ satisfies

$$(\xi f f')' + \tfrac{1}{2}\xi^2 f' = 0 \quad \text{and} \quad f(1) = 0. \tag{3.3a, b}$$

As we shall see in § 4, an important feature of the solution is that

$$f \sim [-A \ln \xi]^{1/2} \quad \text{as} \quad \xi \to 0, \tag{3.4}$$

where A is a constant, found numerically to be about 0.179.

The self-similar early-time stage is followed by an intermediate stage initiated when the current first reaches the sink, as illustrated in figure 2(*a*, *b*). The impact of the sink on the form and evolution of the current is immediate. Once the current has propagated over the sink, fluid begins to leak out of the system, giving rise to an asymmetry of the current; the extent of the current is strongly reduced in the direction of the sink, but remains largely unaffected on the other side of the source.

In the late stages of the current's evolution, the extent of the current becomes very much larger than the distance between the source and the sink, and in this limit the outer profile (far from the source–sink pair) becomes effectively axisymmetric once again (figure 2*c*, *d*). This outer current is fed from a quasi-steady inner region in which flow from the source is partly balanced by leakage through the sink, leaving a residual flux which propagates into the outer current (see figure 5). Indeed the form of the outer solution retains much of the character of the initial self-similar spreading as shown by the profiles in figure 3(*a*). Observations of the profiles in figure 3 contain the genesis of the asymptotic method which we describe in the following section.

A quantity that is of considerable interest from a practical point of view, and is characteristic of the approach to this asymptotic state, is the 'efficiency of storage' which measures the difference between the flux into the reservoir and the leakage flux, with this difference normalized by the input flux. The efficiency of storage is a measure of the fluid that can be permanently stored. In dimensionless variables, the input flux is 1 and the leakage flux is $\Lambda\bar{h}$. We therefore define the efficiency of storage as

$$E_S \equiv 1 - Q_L = 1 - \Lambda\bar{h} = Q_R, \tag{3.5}$$

where the dimensionless residual flux Q_R is the flux of the fluid that passes into the far field and hence is retained within the porous medium. The instantaneous efficiency of storage is plotted in figure 4 for various values of Λ, which shows the essential character of the system: as the strength of the sink (characterized by Λ) is increased, the efficiency of storage declines more rapidly. However, for $\Lambda \gg 1$ the efficiency of storage becomes independent of the strength of the sink. To gain further insight into these numerical results, we now consider the long-time behaviour of the system using asymptotic methods which are related pedagogically to those used in the two-dimensional case by Pritchard (2007) and Neufeld *et al.* (2009).

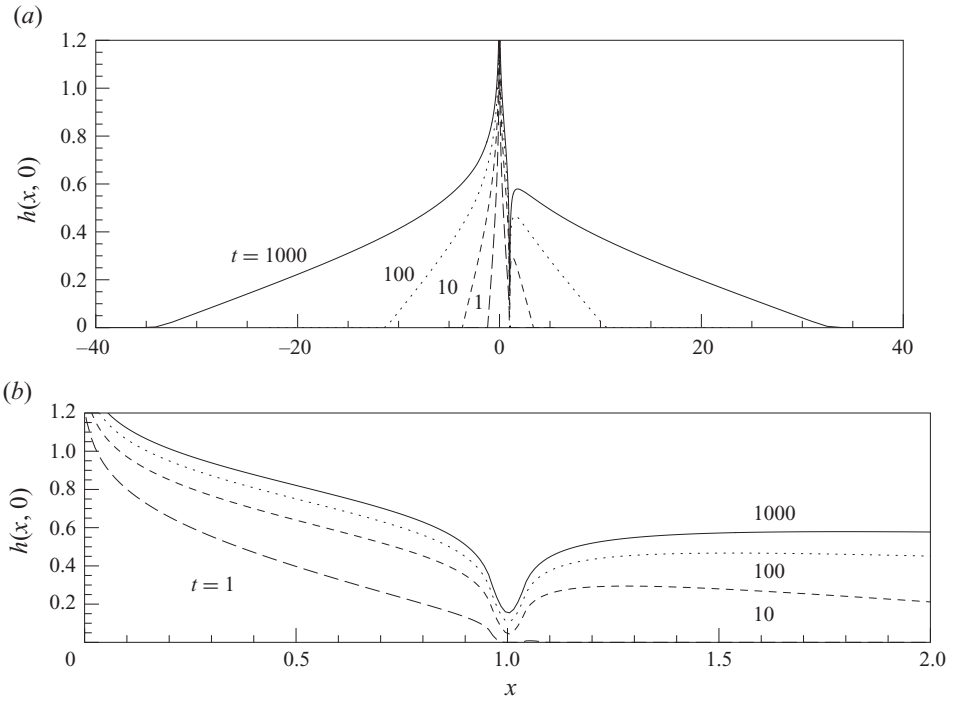

FIGURE 3. Evolution of the current profile $h(0, y)$ for $\Lambda = 2$ and $\epsilon = 0.036$ at times $t = 1$ (long-dashed), 10 (short dashed), 100 (dotted) and 1000 (solid). The full profile in (a) shows the form of the spreading solution far from the source–sink pair, while the profile in (b) shows that the region around the source–sink pair appears to approach a quasi-steady state for $t \gg 1$.

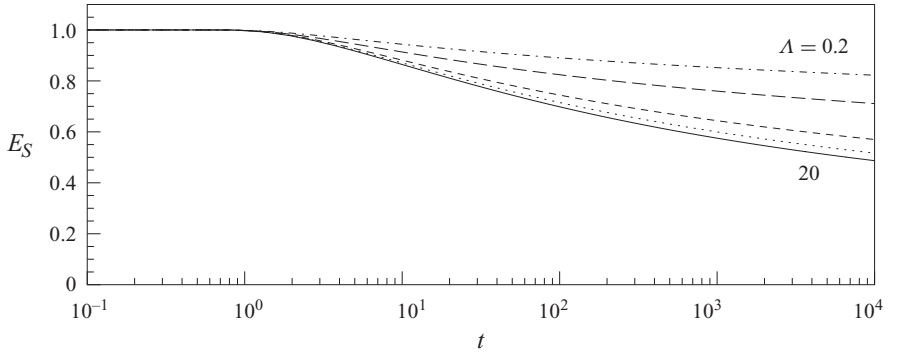

FIGURE 4. Time-dependent efficiency of storage, E_S, for $\Lambda = 0.2$ (dash-dotted), 0.4 (long dashed), 1 (short dashed), 2 (dotted) and 20 (solid) and $\epsilon = 0.036$. In each case, $E_S = 1$ until $t = 0.75$, at which point the current reaches the sink and drainage begins.

4. Long-time asymptotics

We consider the behaviour of the system at long times with the primary aim of determining the asymptotic efficiency of storage. In the long-time limit, we show that the system reaches a quasi-steady state in the region close to the source–sink pair. The quasi-steady state is characterized by a unit input flux and a flux Q_L into the sink. The quasi-steady inner region feeds an evolving axisymmetric gravity current in

the outer region. In turn, the evolution of the flux Q_R into the outer current drives the slow evolution of $Q_L = 1 - Q_R$. In what follows, we first solve for the structure of the inner source–sink region analytically, and then discuss the axisymmetric outer region and the matching procedure. This analysis provides the asymptotic behaviour for such geophysically relevant quantities as the efficiency of storage.

We note that the quasi-steady inner solution depends to some extent on the structure of the flow near a sink of finite radius ϵ. Since $\epsilon \ll 1$, we make the simplifying assumption that variations in the height of the flow above the sink are negligible. This completes the description of the steady inner region. The overall structure of the flow, and hence the efficiency of storage, is then determined by the coupling between inner and outer regions. Finally, we point the interested reader to Appendix B, where we relax the assumption that variations in the height of the flow above the sink are negligible. We find that this distinction somewhat improves the accuracy of the long-term estimate of the efficiency of storage, but does not change the fundamental point that the overall structure is governed by the coupling between inner and outer regions.

4.1. *Inner solution*

In the long-time limit, an inner region around the source and sink becomes quasi-steady. The flux from the source either flows into the sink or flows outward into the spreading current. Therefore, we expect the inner region to obey the steady version of (2.5) for the surface height, namely

$$\tfrac{1}{2}\nabla^2 h^2 = 0, \tag{4.1}$$

with a source of strength $Q = 1$ at the origin and a quasi-steady sink strength $Q_L(t)$. Critically, (4.1) is a linear equation for h^2 and we may use superposition to construct a model for a source–sink pair. For a single source of strength Q located at $r = 0$, the expected profile would be given in radial coordinates by

$$\frac{1}{2}h^2 = -\frac{Q}{2\pi}\ln r + c, \tag{4.2}$$

where c is a constant. For a source–sink pair with a source of strength $Q = 1$ at $z = 0$ and a point sink of strength $Q_L = 1 - Q_R$ at $\zeta = 1$, as shown schematically in figure 5, we might try the superposition

$$\frac{1}{2}h^2 = -\frac{1}{2\pi}\ln|\zeta| + \frac{1-Q_R}{2\pi}\ln|\zeta - 1| + c, \tag{4.3}$$

though this expression gives negative values of h^2 sufficiently close to $\zeta = 1$. However, we are interested in a finite-size circular sink centred on $\zeta = 1$ rather than a point sink at $\zeta = 1$. We can use the method of images to adapt (4.3) slightly so that the height takes a uniform value h_1 at the edge $|\zeta - 1| = \epsilon$ of the sink, and thus obtain

$$\frac{1}{2}h^2 = \frac{1}{2\pi}\ln\left|\frac{\zeta - (1-\epsilon^2)}{\epsilon\zeta}\right| - \frac{Q_R}{2\pi}\ln\frac{|\zeta - 1|}{\epsilon} + \frac{1}{2}h_1^2 \quad \text{in} \quad |\zeta - 1| > \epsilon. \tag{4.4}$$

The image system here consists of a point sink of strength 1 at $\zeta = 1 - \epsilon^2$ and a point source of strength Q_R at $\zeta = 1$, both of which are within the perimeter of the actual physical sink. Similar image systems occur in problems in inviscid hydrodynamics, such as a line vortex outside a cylinder, and in electrostatics.

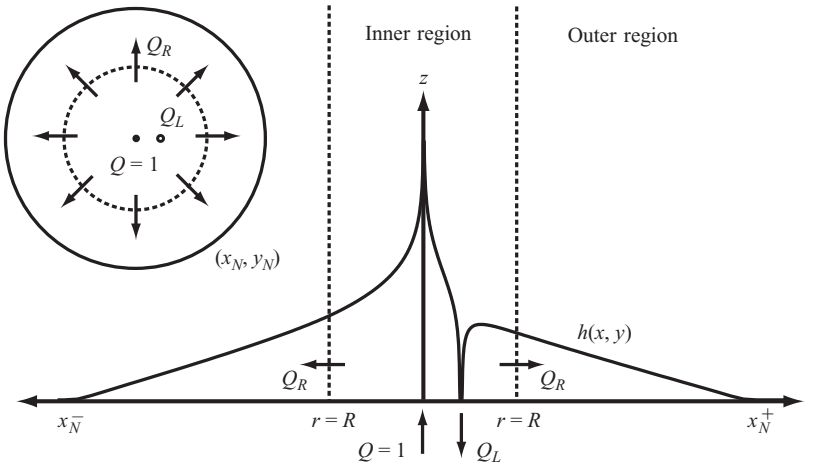

FIGURE 5. At long times the inner region reaches a quasi-steady state in which the source flux Q is balanced by a slowly evolving sink flux $Q_L(t)$ and residual flux $Q_R(t)$. This residual flux feeds an expanding axisymmetric current of extent (x_N, y_N).

Anticipating that we will match the outer limit of the inner profile (4.4) to a model of a spreading axisymmetric current (derived in § 4.2), we note that in the limit $|\zeta| \gg 1$

$$\frac{1}{2}h^2 \sim -\frac{Q_R}{2\pi}\ln|\zeta| + \frac{1-Q_R}{2\pi}\ln\left(\frac{1}{\epsilon}\right) + \frac{1}{2}h_1^2 + O\left(\frac{1}{\zeta}\right). \tag{4.5}$$

Equations (4.4) and (4.5) are completed with a model of flow within the sink that determines the height, h_1, at the edge. We focus our attention on this problem in § 4.3.

We conclude by noting the analogy between the steady-state flow in the inner region and an electrostatic field, which arises from the fact that (4.1) is equivalent to Laplace's equation for an effective electric potential $\varphi \equiv h^2/2$. Under this analogy, in the present problem the source of flux corresponds to a line charge of strength $Q = 1$ while the sink corresponds to a cylindrical conductor with a constant potential and a total charge of strength Q_L. The solution in electrostatics is then analogous to that given in (4.4) (see, for example, Bleaney & Bleaney 1976). The analogy can be applied in other geometries where the electrostatic problem is amenable to solution (see Vella *et al.* 2010).

4.2. *Outer solution*

We now turn our attention to the outer spreading gravity current that is fed from the inner region (figure 5). Both the numerical solutions and the form of (4.5) suggest that, at long times and large distances from the source–sink pair, the current is axisymmetric at leading order. From (4.5), the height where the current matches to the inner region depends on time only through the evolution of the flux $Q_R(t)$.

We first note that the similarity solution (3.2) for a gravity current fed by a constant flux has a height that is independent of time at a fixed value of the similarity coordinate ξ. However, a fixed radius r corresponds to a decreasing value of ξ and hence, from (3.4), the near-source height of a constant-flux current varies logarithmically with time. This observation suggests that the solution for a spreading outer current fed by a source region of the form (4.5) can be found by assuming that the source flux Q_R also varies logarithmically with time. Importantly, logarithmic variations are much slower than the $t^{1/2}$ diffusive spreading, and this allows for an asymptotic solution.

We seek a solution to

$$\frac{\partial h}{\partial t} = \frac{1}{r}\frac{\partial}{\partial r}\left(rh\frac{\partial h}{\partial r}\right), \tag{4.6}$$

subject to the boundary condition

$$-2\pi r\, h\frac{\partial h}{\partial r} \to Q_R \quad \text{as} \quad r \to 0, \tag{4.7}$$

where Q_R is an algebraic function of $\ln t$. Since Q_R is only slowly varying, we posit that the solution resembles the self-similar solution for a constant flux, and make a change of variables

$$h \equiv Q_R(s)^{1/2} f(s, \eta), \tag{4.8}$$

where

$$s \equiv \ln t \quad \text{and} \quad \eta \equiv \frac{r}{Q_R(s)^{1/4} t^{1/2}}. \tag{4.9a, b}$$

We substitute (4.8) and (4.9) into (4.6) and (4.7) to obtain, without approximation,

$$\frac{\eta}{2}\frac{\partial f}{\partial \eta} + \frac{1}{\eta}\frac{\partial}{\partial \eta}\left(\eta f\frac{\partial f}{\partial \eta}\right) = \left(\frac{f}{2} - \frac{\eta}{4}\frac{\partial f}{\partial \eta}\right)\frac{1}{Q_R}\frac{\partial Q_R}{\partial s} - \frac{\partial f}{\partial s} \tag{4.10}$$

and

$$-2\pi\eta f\frac{\partial f}{\partial \eta}\bigg|_{\eta\to 0} = 1. \tag{4.11}$$

The factor $t^{1/2}$ in (4.9*b*) accounts for most, but not all, of the time-dependence in f. Thus, the right-hand side of (4.10) is $O(1/s)$ as $t \to \infty$ and may therefore be neglected at leading order by comparison with the left-hand side. The remaining problem for f is independent of the time-like variable s and the left-hand side of (4.10) is identical to (3.3*a*). The solution is thus the same as the similarity solution for a constant-flux current as summarized in (3.1)–(3.4), though with the radial similarity coordinate normalized to give unit flux rather than unit radius. Hence, the solution of (4.6) and (4.7) with slowly varying Q_R is given at leading order by the similarity solution for the instantaneous value of Q_R; the variation of Q_R only appears through $O(1/\ln t)$ corrections. The form of $Q_R(t)$ is determined by matching at leading order to the inner region.

As $\eta \to 0$ the solution of (4.10) and (4.11) obeys

$$f \sim (-\ln \eta/\pi)^{1/2}. \tag{4.12}$$

Thus, the inner limit of the outer spreading current is given by

$$\frac{1}{2}h^2 = -\frac{Q_R}{2\pi}\ln\left(\frac{r}{Q_R^{1/4}t^{1/2}}\right), \tag{4.13}$$

and it is this height that must now be matched to the quasi-steady inner profile described in § 4.1 to complete our model of the long-time structure of the current.

4.3. *Asymptotic efficiency of storage*

The long-time behaviour of the efficiency of storage and the profile of the current can now be calculated by matching the inner quasi-steady profile to the axisymmetric spreading outer profile. By equating (4.5) with (4.13) we find

$$\frac{Q_R}{2}\left[\frac{1}{2}\ln Q_R + \ln t\right] = (1 - Q_R)\ln\left(\frac{1}{\epsilon}\right) + \pi h_1^2. \tag{4.14}$$

To complete our analysis of the long-term efficiency of storage, we require a model of the height at the edge of the sink. Motivated by the simplicity of the resulting analysis, we approximate the profile within the sink by its average value, $\overline{h}$, given in (2.9). The flux through the sink is thus $\Lambda h_1 \simeq \Lambda \overline{h}$ and we therefore find that

$$h_1 = \frac{Q_L}{\Lambda} = \frac{1 - E_S}{\Lambda}. \tag{4.15}$$

We substitute this model for the height at the sink into the matching condition (4.14) between inner and outer regions, and use the fact that the efficiency of storage is defined by $E_S = 1 - Q_L = Q_R$. In this way, the desired equation for the efficiency of storage

$$\ln t = 2\frac{(1 - E_S)}{E_S} \ln\left(\frac{1}{\epsilon}\right) + \frac{2\pi}{\Lambda^2}\frac{(1 - E_S)^2}{E_S} - \frac{1}{2}\ln E_S \tag{4.16}$$

is obtained, which gives E_S implicitly as a function of time and the two dimensionless parameters that describe the sink size and strength.

In the very-long-time limit of large $\ln t$, (4.16) predicts that $E_S \ll 1$ and we can simplify further to

$$E_S = \frac{c_S}{\ln t} + O\big(E_S^2 \ln E_S\big), \tag{4.17}$$

with the constant c_S defined explicitly in terms of the geometry and strength of the sink as

$$c_S = 2\ln\left(\frac{1}{\epsilon}\right) + \frac{2\pi}{\Lambda^2}. \tag{4.18}$$

The very-long-time behaviour in (4.17) clearly requires $\ln t \gg c_S$ for $E_S \ll 1$. For $\epsilon = 0.036$ and $\Lambda = 1$, for example, this gives $\ln t \gg 12.9$ and, even as $\Lambda \to \infty$, we require $\ln t \gg 6.6$. It follows that the approach to the asymptotic (4.17) is slow, occurring on a very much longer time scale than the $O(1)$ time scale for the flow to reach the sink. It is worth emphasizing that the efficiency of storage does decay to zero as $t \to \infty$, as was the case in the two-dimensional geometry studied by Neufeld *et al.* (2009). However, it is interesting that the logarithmic decay of E_S found here is significantly slower than the algebraic decay observed in two dimensions or with a line sink (see Vella *et al.* 2010). Because of the slow approach to (4.17), we use (4.16), which requires only $t \gg 1$, to estimate efficiencies in our application to storage of CO_2 in § 5.

A comparison of the predicted coefficient c_S with the results of the full numerical calculations is shown in figure 6, and is constructed in the following way. We first note that though the numerical calculations are typically run to $t \sim 10^4$, the time at which $E_S \ll 1$ may be large and so higher-order terms may still play a significant role. Motivated by (4.16) we fitted the numerically calculated efficiency of storage (as shown in figure 4) to a function of the form

$$\ln t = \frac{m_1}{E_S} + m_2 + m_3 \ln(E_S) + m_4 E_S. \tag{4.19}$$

This enables us to extract the asymptotic nature of the solution and test the long-time limit (4.17) while accounting for leading-order corrections to the behaviour at intermediate times. As is clear from the comparison in figure 6, the assumption of constant height above the sink, while apparently rather crude, is able to predict accurately the dominant asymptotic behaviour as a function of Λ. Thus, a model that roughly captures drainage at the sink, but provides an accurate matching of the

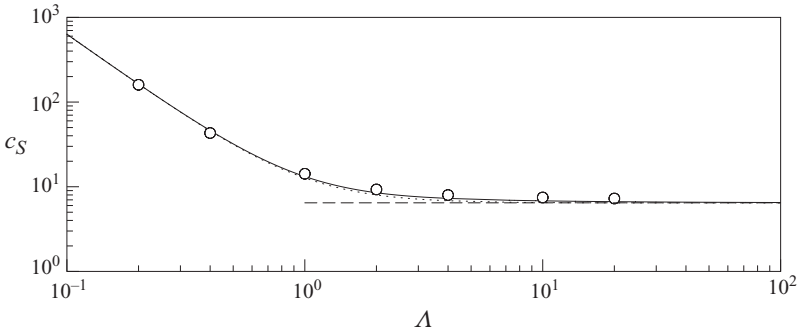

FIGURE 6. The coefficient of storage c_S as a function of Λ for $\epsilon = 0.036$. The coefficients fitted from numerical solutions to the full evolution equations (2.5)–(2.7) are shown by circles. The dotted curve shows the prediction using a uniform sink height as in (4.16) while the solid curve shows the prediction of Appendix B, in which the profile within the sink is resolved. The limit $\Lambda \to \infty$, in which $h_1 \to 0$, is shown by the dashed line and is given by $c_S = 2\ln(1/\epsilon)$, as shown by (4.18).

quasi-steady source–sink flow to the evolving axisymmetric current, produces a viable model of the efficiency of storage in underground reservoirs.

To determine the importance of the profile immediately above the sink, a quasi-steady model resolving an axisymmetric profile within the sink has also been constructed (details can be found in Appendix B). The results of this more detailed model are also shown in figure 6. We find that the difference in the estimated efficiency of storage between the simple sink-averaged theory and the detailed model is always less than 6.5 % for the values of Λ and ϵ considered here. This gives us confidence that the solution presented above captures the essential details of the process and is relatively insensitive to the details of the dynamics within the sink itself. Therefore, while the specifics of the near-sink region may merit further study, we do not expect these to unduly affect the results detailed here.

5. Discussion of leakage from geological carbon-dioxide storage sites

Recently, the storage of large volumes of CO_2 within the subsurface has received much attention as a possible means of mitigating anthropogenic emissions of this greenhouse gas leading to climate change (Pacala & Socolow 2004). In typical carbon capture and storage (CCS) schemes, CO_2 is first captured at a stationary source such as a coal-fired power station, and then compressed for injection into the subsurface. The CO_2 is typically injected at depths greater than 1000 m where, under representative reservoir temperatures and pressures, it is a supercritical liquid. The injected CO_2 is typically much less dense than the ambient fluid within the reservoir (often brine in saline aquifers) and therefore rises vertically through the available pore space until it reaches a relatively impermeable layer or cap rock, where it spreads horizontally due to the buoyancy contrast with the surrounding fluid. Thus, in the early stages of injection, it is the presence of an impermeable cap rock which enables stable storage of CO_2 within the subsurface.

As injection proceeds, and indeed once injection has ceased, a number of secondary processes may become important in immobilizing the CO_2 on time scales of order a thousand years. These processes include, but are not limited to, dissolution of CO_2 into the ambient reservoir fluid leading to dense (and therefore stably stored)

CO_2-saturated fluid, residual trapping of CO_2 within the small pore spaces of the host rock due to the effects of surface tension, and the ultimate mineralization of injected CO_2 through reactions with the host rock. However, as all these processes require some time before the stably trapped volume of CO_2 is comparable with the volume injected, it is the integrity of the cap rock that determines the efficiency of storage on short time scales. Our calculations therefore address the effect of imperfections in the bounding impermeable barrier on the ability of the reservoir to sequester CO_2 long enough for secondary processes to immobilize the injected CO_2 permanently.

We can begin to assess the impact of a sink on the efficiency of storage in a variety of reservoirs by considering the time, t_{90}, taken for the efficiency to fall to 90 %. An estimate of this time scale can be readily constructed by combining the simple model in which there is a constant fluid depth above the sink with the asymptotic behaviour as $\Lambda \to \infty$. At the efficiency of storage $E_S = 0.9$ we find the dimensionless estimate

$$t_{90} = (10/9)^{1/2}\epsilon^{-2/9}\exp(\pi/45\Lambda^2) \geqslant (10/9)^{1/2}\epsilon^{-2/9} \tag{5.1}$$

from (4.16), which agrees with our full numerical results to within 16 % for $\Lambda \geqslant 0.5$. We note that for $\epsilon \ll 1$, t_{90} is much larger than the time taken for the current to reach the sink.

The worst-case scenario is $\Lambda \gg 1$ given by the inequality above, in which case there is negligible resistance to flow within the sink, and leakage rates are determined by the flux of fluid through the current to the border of the sink. Such a situation may arise if an abandoned well-head some distance from the point of injection allows rapid leakage, and possibly decompression of CO_2 as it escapes from the reservoir. In this limit of rapid leakage ($\Lambda \to \infty$), the efficiency of storage reaches 90 % at a dimensional time

$$\tilde{t}_{90} \approx \frac{x_S^{20/9}}{r_S^{2/9}}\left(\frac{\phi\mu}{qkg\Delta\rho}\right)^{1/2}. \tag{5.2}$$

We can estimate the magnitude of $\tilde{t}_{90}$ for representative reservoir conditions in the following way. The viscosity and density differences do not vary appreciably between aquifers. For example, values typical of the large-scale demonstration project at Sleipner are $\mu = 4.5 \times 10^{-5}\,\mathrm{Pa\,s}$, $g = 9.81\,\mathrm{m\,s^{-2}}$, $\Delta\rho = 505\,\mathrm{kg\,m^{-3}}$, $\phi = 0.03$ and $q = 1\,\mathrm{MT\,yr^{-1}} \simeq 0.062\,\mathrm{m^3\,s^{-1}}$ (see Bickle *et al.* 2007). However, the permeability can vary by orders of magnitude, and similarly the position of any leakage points with respect to the injection well will vary greatly from one site to another. Figure 7 shows the lower bound (5.2) for the dimensional time $\log_{10}(\tilde{t}_{90})$ (days) as a function of the permeability k ($\mathrm{m^2}$) of the host reservoir and distance to the leakage point x_S (m). We see that the time over which the efficiency of storage decays to 90 % varies greatly with distance to the injection well, from 10–10^5 days, for distances from 100 m to 10 km.

The utility of the leakage calculations is immediate: an estimate can quickly be made of the magnitude and time scale for leakage from the subsurface. Moreover, by examining (5.2), or more generally (4.16), we can estimate the extent of the cap rock x_S that must be free from fissures of typical extent r_S to ensure an efficiency of storage greater than E_S over a time scale t. In this way, calculations of the long-time storage efficiency can be used to estimate the extent of leakage and to guide site selection. Such estimates are essential given the total volume of CO_2 which needs to be sequestered within the subsurface to have a significant effect relative to current anthropogenic emissions. These large volumes will undoubtedly sample much of the subsurface during the lifetime of any injection project, and in so doing may encounter

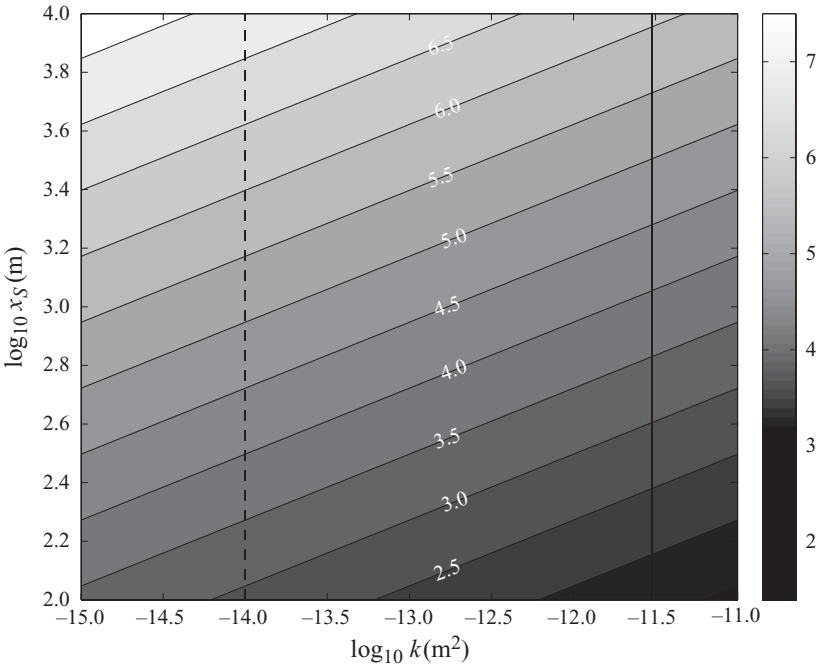

FIGURE 7. A contour plot showing $\log_{10}(\tilde{t}_{90}[\text{days}])$, the time scale over which the efficiency of storage $E_S = 0.9$, as a function of the permeability of the host reservoir $k\,(\text{m}^2)$ and the distance from the source to the sink $x_S\,(\text{m})$ as given in (5.2). Calculations assume a typical sink size for a large bore hole, $r_S \simeq 0.5\,\text{m}$. For comparison, we plot estimates of the permeability of the Sleipner reservoir (vertical solid line) and the Alberta basin (vertical dashed line).

faults, fractures, previously drilled wells and any other geological feature which allows leakage through the bounding cap rock.

6. Conclusions

We have analysed the buoyancy-driven propagation of fluid within a porous medium bounded by an impermeable layer and calculated the rate at which it may escape through a single localized sink. The dimensionless governing equations for buoyancy-driven flow through the reservoir and leakage through the sink presented in § 2 were solved both numerically and analytically and the results are reported in §§ 3 and 4. The behaviour of such currents can be characterized by an efficiency of storage E_S. We find that the efficiency of storage is dependent on only two dimensionless parameters: the characteristic size of the sink ϵ and the strength (or permeability) of the sink Λ defined by (2.8).

Importantly, we find in both our numerical results and our analysis that the efficiency of storage obeys

$$E_S \propto \frac{1}{\ln t} \tag{6.1}$$

in the long-time limit, with the constant of proportionality $c_S(\epsilon, \Lambda)$ depending only on the characteristic size and strength of the sink. In practice, this implies that leakage from a reservoir with a point source and sink decays much more slowly than in the

analogous two-dimensional problem (Neufeld *et al.* 2009), where

$$E_{S,2d} \propto t^{-1/2}. \tag{6.2}$$

Furthermore, the results of § 5 suggest that the time needed to reach 90 % efficiency within a typical reservoir vary greatly with distance between the injection point and the sink (see figure 7).

Finally, we note the utility of the approach outlined here to a number of related studies. In particular, the asymptotic analysis presented in § 4 is based, at its heart, on the realization that, for currents in which leakage occurs, a quasi-steady inner region develops, which is coupled to a slowly spreading outer region. A number of implications for more complex cases, which may be found within the environment, follow. Because the inner region is in a quasi-steady state, and therefore governed by a linear equation (4.1) for the surface profile, the present analysis can be extended in a straightforward way to include multiple leakage wells, a case which may be of relevance to such geological settings as the Alberta basin (Nordbotten *et al.* 2009). The method has also been brought to bear on the related problem of injection from a point source and leakage through a linear fracture or fault by Vella *et al.* (2010) where the efficiency of storage was found to decay algebraically in time ($E_S \propto t^{-2/5}$). Future extensions of this work on leakage will address the finite depth of geological reservoirs, and the finite period over which injection is anticipated. However, in addition to CO_2 sequestration, there are a number of other applications where this technique may be usefully applied. In particular, we note that the analysis above, focusing on the spread of a buoyant fluid within a porous medium, may also be applied to the flow of viscous fluids on a surface with leakage. Therefore, the methodology not only provides an effective tool for evaluating leakage in geological carbon sequestration projects but also provides the method with which to study a series of related porous and viscous problems within the environment and industry.

J.A.N. is grateful for support through a Lloyd's Tercentenary Fellowship and a Leverhulme Early Career Fellowship. D.V. is supported by a research fellowship from the 1851 Royal Commission and an Oppenheimer Early Career Research Fellowship. Partial support of the research of H.E.H. comes from a Wolfson Royal Society merit award. We are grateful to all these funding agencies.

Appendix A. Numerical method

The numerical solutions to (2.5) were computed using the following finite-difference scheme. A rectangular, but non-uniform, grid was used to divide the computational domain into an array of rectangular cells. The point source was approximated by a single cell and the circular sink by a cluster of 20 cells centred on $(1, 0)$, as shown schematically in figure 8. The effective sink radius ϵ_e was estimated from its area as

$$\epsilon_e = \left(\frac{40\Delta_0^2}{\pi}\right)^{1/2} \approx 0.036, \tag{A 1}$$

where $\Delta_0 \approx 0.01$ is the uniform size of the square cells in this region.

The height of the current was represented by the values at the centre of each cell, but the diffusivity h in the nonlinear diffusion operator $\nabla \cdot (h\nabla)$ was evaluated at the edges of the cells using linear interpolation between the central values. Equation (2.5) was thus discretized in a flux-conservative manner by considering the fluxes across each cell edge, and in the source and sink, during each time step.

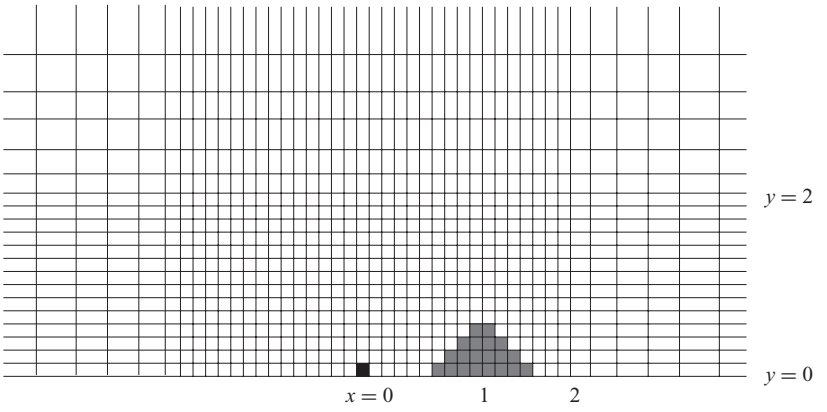

FIGURE 8. A schematic representation of the grid spacing around the source–sink pair. The sink is resolved by a 20 cell pattern arranged to roughly approximate a cylindrical fissure in the cap rock. Note that distances are not to scale, and the number of grid cells is only illustrative.

Time-stepping was performed using the alternating-direction-implicit (ADI) method of generalizing the Crank–Nicolson scheme to two dimensions (see Press *et al.* 1997, § 19.3). The nonlinear diffusivity was estimated at the middle of the time step by first taking a predictor time step with the present diffusivity, and then averaging the present and the predicted diffusivity for the actual time step. Except above the sink, where the leakage was evaluated fully implicitly, the time-stepping was thus second-order accurate. The time step was chosen adaptively using a criterion based on the sum of squared differences between a full time step and two half time steps.

In order both to resolve the structure of the profiles around the source and sink and to simulate a spreading current with ever-increasing radius, we implemented a variable spatial resolution (figure 8). A uniform and constant grid spacing $\Delta_0 \approx 0.01$ was used in the region $|x|, |y| \leqslant 2$. Outside this region, the grid spacing was increased smoothly in each of the x- and y-directions using a functional stretching of the form

$$\Delta_i = \Delta_0 + c\left[1 + \tanh\left(\frac{i - 51}{10}\right)\right], \tag{A 2}$$

where $i = 1, 2, \ldots, 100$ is an index in the relevant direction beyond $|x| = 2$ or $|y| = 2$. The constant c determines the magnitude of the stretching of the grid, and the smooth variation allows the spatial differencing also to be second-order accurate. In order to simulate a spreading current over many decades of evolution in time, we doubled the size of c, thus increasing the domain size, whenever the extent of the current reached within 75 % of the edge of the domain. On each such occasion, the current was interpolated onto the new grid using a scheme that conserved the local volume. The outer part of the grid stretches in proportion to the radial extent of the current and thus maintains an appropriate resolution of the self-similar outer solution, while the inner part maintains resolution near the source and sink. The numerical solutions reported were based on a grid of about 600×300 cells (with symmetry about $y = 0$); sample calculations with different resolution, and with variation of the time-step control, exhibited negligible differences.

Appendix B. Resolving the current profile above the sink

B.1. *Axisymmetric profile above the sink: small Λ*

The long-term efficiency of storage depends on the behaviour of the flow above the sink and in general is given by (4.14). We found in § 4.3 that an average of the profile above the sink adequately predicts the efficiency of storage (as shown in figure 6). Here we introduce a model that resolves the profile above the sink assuming the form of drainage given by (2.1). We consider radially symmetric, quasi-steady leakage driven by the height of the fluid layer above the sink. This approximation neglects the weak azimuthal variation around the sink, and therefore the magnitude of leakage is given by

$$\lambda h = \frac{1}{\tilde{r}}\frac{\mathrm{d}}{\mathrm{d}\tilde{r}}\left(\tilde{r}h\frac{\mathrm{d}h}{\mathrm{d}\tilde{r}}\right), \tag{B 1}$$

where $\tilde{r}$ is the local radial coordinate centred on the sink. Equation (B 1) must be solved subject to the conditions

$$h'(0) = 0 \quad \text{and} \quad 2\pi\int_0^{\epsilon} \tilde{r}\lambda h \, \mathrm{d}\tilde{r} = Q_L. \tag{B 2a, b}$$

These conditions correspond to axisymmetry (about the axis of the sink) and impose a fixed total leakage Q_L, respectively.

The solution of (B 1) and (B 2a, b) can be rescaled using h_0, the as-yet-unknown height at $\tilde{r} = 0$, onto a universal function that describes the profile above the sink. An auxiliary condition then determines the value of h_0 from Q_L, ϵ and Λ. We define $R = \tilde{r}/\sqrt{h_0/\lambda}$ and $H(R) \equiv h/h_0$ so that

$$H = \frac{1}{R}\frac{\mathrm{d}}{\mathrm{d}R}\left(RH\frac{\mathrm{d}H}{\mathrm{d}R}\right), \tag{B 3}$$

$$H(0) = 1 \quad \text{and} \quad H'(0) = 0. \tag{B 4a, b}$$

The solution $H(R)$ of (B 3) subject to (B 4a, b) does not involve any of the governing parameters and as such is a universal function. The numerical solution is shown in figure 9(a) along with the asymptotic behaviour for large and small R,

$$H \sim \begin{cases} 1 + R^2/4, & (R \ll 1), \\ R^2/8, & (R \gg 1), \end{cases} \tag{B 5a, b}$$

which reproduces the behaviour of $H(R)$ very well in the appropriate limits.

The total flux condition (B 2b) may be rewritten using (B 1) in terms of the boundary flux. After scaling, we have

$$2\sqrt{\pi}h_0^{3/2}H(R_S)H'(R_S) = \frac{Q_L}{\sqrt{\Lambda}}, \tag{B 6}$$

where

$$R_S = \frac{\epsilon}{\sqrt{h_0/\lambda}} = \left(\frac{\Lambda}{\pi h_0}\right)^{1/2} \tag{B 7}$$

is the rescaled radius of the sink. In this form (B 6) implicitly determines h_0 from Q_L and Λ. We can further use the asymptotic behaviour (B 5a, b) to ascertain two limiting forms for h_0. For $R_S \ll 1$ the profile above the sink is relatively constant, and thus to leading order

$$h_0\Lambda = Q_L, \tag{B 8}$$

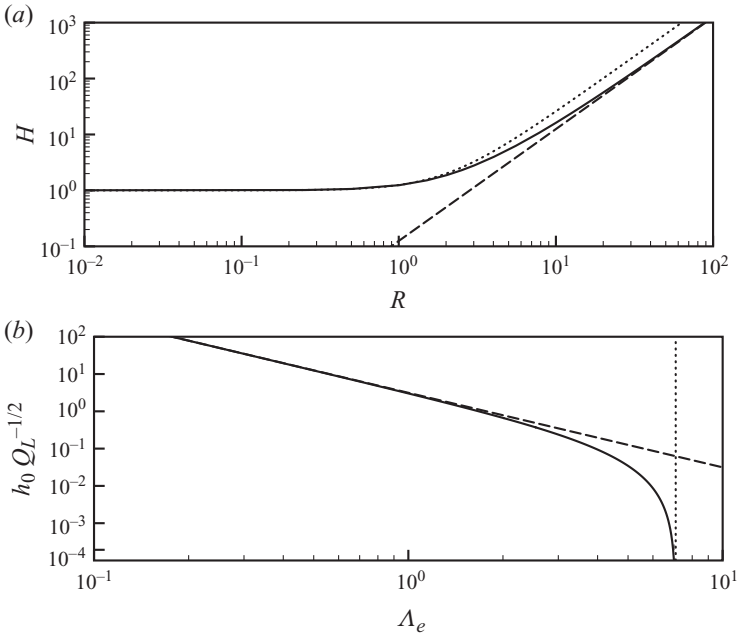

FIGURE 9. (*a*) The rescaled profile within the sink $H(R)$ as a function of the scaled radial position. The solid curve shows the numerical solution of (B 3), the dotted curve shows the asymptotic result (B 5*a*), valid for $R \ll 1$, and the dashed line shows the asymptotic result (B 5*b*), valid for $R \gg 1$. (*b*) The profile scaled by the height h_0 at the centre of the sink as a function of the grouping $\Lambda Q_L^{-1/2}$. The limit $\Lambda Q_L^{-1/2} \ll 1$ is shown by the dashed line and the upper bound $\Lambda Q_L^{-1/2} = 4\pi^{1/2}$, at which a dry spot forms in the middle of the sink, is shown by the dotted line.

while for $R_S \gg 1$ we find that

$$\Lambda = 4\sqrt{\pi Q_L}. \tag{B 9}$$

This implies that the height at the centre of the sink decreases towards zero until condition (B 9) is met and a dry spot develops in the midst of the sink. We emphasize that this dry spot is not due to the effects of surface tension but simply reflects an insufficient boundary flux Q_L to maintain drainage over the entire sink. Figure 9(*b*) shows the rescaled height at the centre of the sink $h_0/Q_L^{1/2}$ as a function of an effective sink strength, which we define as

$$\Lambda_e \equiv \frac{\Lambda}{Q_L^{1/2}}. \tag{B 10}$$

B.2. *Large Λ: dry spot*

The results above suggest that there are no solutions with $h_0 \neq 0$ for $\Lambda_e > 4\pi^{1/2} \simeq 7.1$ and we conclude that a dry spot must develop, i.e. there is a radius r_d such that $h = 0$ for $r < r_d$. Here we calculate the radius of the dry spot r_d and the current depth for $r_d < r < \epsilon$. Again, the profile of the current is governed by (B 3), now with boundary conditions

$$h(r_d) = 0, \quad 2\pi h(r_d)h'(r_d) = 0, \quad \text{and} \quad 2\pi \int_{r_d}^{\epsilon} \lambda h r \, \mathrm{d}r = Q_L, \tag{B 11a, b, c}$$

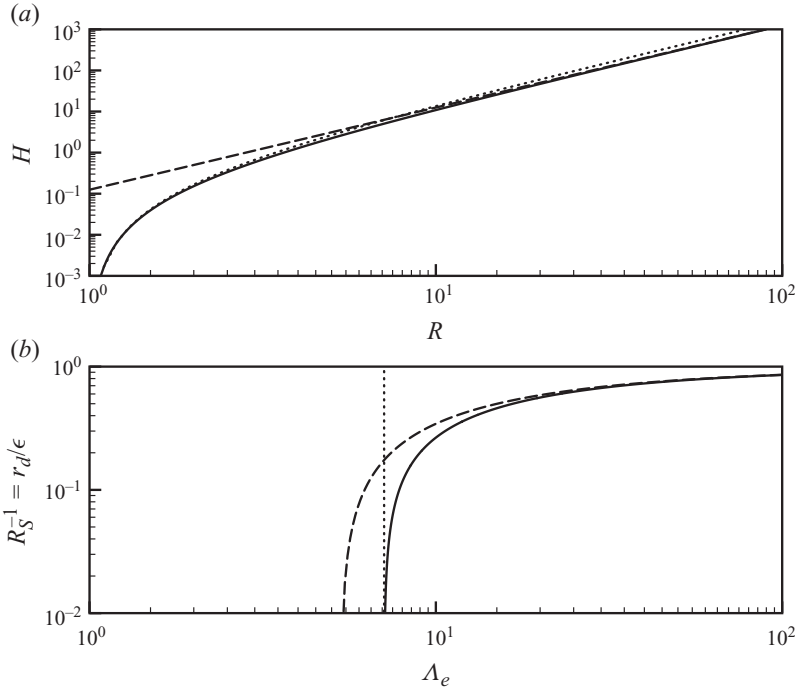

FIGURE 10. (*a*) The rescaled profile within the sink outside a dry spot $H(R)$. Here, the solid curve shows the numerical solution of (B 3) with boundary conditions (B 13*a, b*). The dotted curve shows the asymptotic result (B 14*a*), valid for $R - 1 \ll 1$, and the dashed line shows the asymptotic result (B 14*b*), valid for $R \gg 1$. (*b*) The dependence of the radius of the dry spot, $R_S^{-1} = r_d/\epsilon$, on Λ_e. Again, the numerical solution is shown by the solid curve while the dotted line shows the critical value at which a dry spot first appears (B 16) and the dashed curve shows the large Λ_e asymptotics (B 17).

which defines the radius of the dry spot, requires zero fluid flux across the inner radius of the dry spot and requires the total flux to be equal to Q_L respectively. Inspired by the previous calculation of a completely wet sink, we now let

$$R \equiv r/r_d \quad \text{and} \quad H \equiv h/\lambda r_d^2. \tag{B 12}$$

With these rescalings, (B 1) again becomes (B 3) but now with boundary conditions

$$H(1) = 0 \quad \text{and} \quad 2\pi H(1)H'(1) = 0. \tag{B 13a, b}$$

These two conditions both define the edge of the dry spot and require zero flux across the radius of the dry spot, respectively. A numerical solution of this system may easily be determined and reproduces the asymptotic results

$$H \sim \begin{cases} (R-1)^2/6, & (R - 1 \ll 1), \\ R^2/8, & (R \gg 1), \end{cases} \tag{B 14a, b}$$

both of which are shown in figure 10(*a*). Having found the height of current above the sink, we now turn our attention to the radius of the dry spot.

The requirement that the flux through the sink be equal to Q_L (B 11) can now be written as

$$\frac{2}{\pi} R_S^{-3} H(R_S) H'(R_S) = \frac{Q_L}{\Lambda^2}, \tag{B 15}$$

where the scaled radius of the sink is defined as $R_S \equiv \epsilon / r_d$. We note that when the radius of the sink is far greater than the radius of the dry spot, $R_S \gg 1$, we again recover

$$\Lambda = 4\sqrt{\pi Q_L}. \tag{B 16}$$

That is, the dry spot appears continuously at the critical value at which the completely wet solution disappears. In contrast, for $R_S - 1 \ll 1$ the radius of the dry spot is nearly coincident with the radius of the sink. In this limit we find, through application of (B 14*a*) to (B 15), that the radius of the dry spot is given by

$$R_S^{-1} = \frac{r_d}{\epsilon} = 1 - \left(\frac{9\pi Q_L}{\Lambda^2}\right)^{1/3} = 1 - \left(\frac{9\pi}{\Lambda_e^2}\right)^{1/3}. \tag{B 17}$$

These two asymptotic results are shown along with the full numerical solution in figure 10(*b*).

B.3. *The height at the edge of the sink*

The calculations presented in §§ B.1 and B.2 now provide a model that resolves the current profile above the sink. Two distinct regimes were found: one in which sufficient fluid is advected towards the sink such that the sink remains completely covered and the other in which a dry spot develops at the centre of the sink. The transition between these regimes depends both on the strength of the sink and the flux of fluid towards it. However, we note from § 4.3 that it is the height at the edge of the sink, h_1, which enables us to calculate the long-term efficiency of storage. This height can be calculated numerically as a function of Λ_e and in the limits of both $\Lambda_e \ll 1$ and $\Lambda_e \gg 1$ analytically.

As we have already seen when $\Lambda_e \ll 1$ the profile within the sink is effectively constant. Thus, the height at the edge of the sink in the limit $\Lambda_e \ll 1$ is $h_1 \, Q_L^{-1/2} \sim \Lambda_e^{-1}$. In contrast, when $\Lambda_e \gg 1$ the majority of the sink is free from liquid with only a thin rim producing the required leakage flux. In this limit, we recall that the profile of the current is asymptotically given by (B 14*a*) with the scaled radius of the edge of the sink given by (B 17). Thus, we find that the height at the edge of the sink in the limit $\Lambda_e \gg 1$ is given by $h_1 / Q_L^{1/2} \sim (3/8\pi\Lambda_e)^{1/3}$. We may summarize these results as

$$\frac{h_1}{Q_L^{1/2}} \sim \begin{cases} \Lambda_e^{-1}, & \Lambda_e \ll 1, \\ \dfrac{1}{2}\left(\dfrac{3}{\pi}\right)^{1/3} \Lambda_e^{-1/3}, & \Lambda_e \gg 1. \end{cases} \tag{B 18a, b}$$

This result completes our description of the efficiency of storage as defined by (4.14) and is plotted in figure 11. Furthermore, the resolved model of the sink provides a highly refined model of the profile within the inner region. The comparison of the inner region between the resolved model, the constant profile within the sink and the numerical solutions as shown in figure 12 highlight the excellent agreement that can be found between the numerical solution and these asymptotic expressions even after a moderately short time ($t = 100$).

Finally, this more detailed model of the height at the edge of the sink enables a revised estimation of the coefficient c_S describing the efficiency of storage for varying model parameters. The results, shown in figure 6 by a solid curve, indicate that the specific model of the sink geometry does not greatly influence the long-term efficiency of storage.

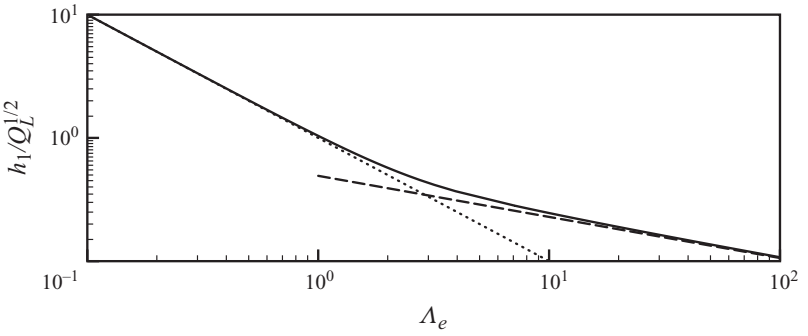

FIGURE 11. Logarithmic plot of the effective sink height, $h_1 Q_L^{-1/2}$, as a function of the effective value of Λ, $\Lambda_e \equiv \Lambda/Q_L^{1/2}$. The results of numerical computations (solid curve) compare well with the asymptotic expressions (B 18*a*) in the limit $\Lambda_e \ll 1$ (dotted) and (B 18*b*) in the limit $\Lambda_e \gg 1$ (dashed).

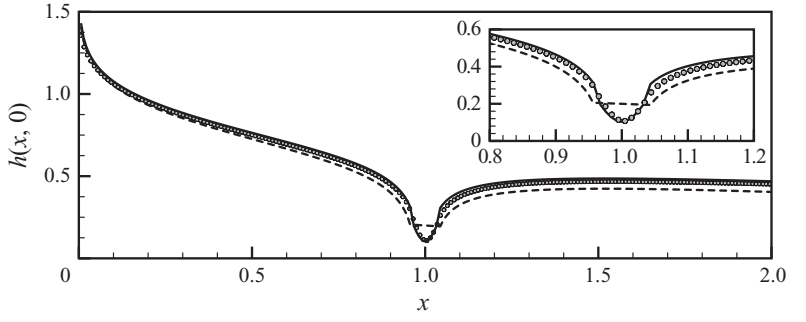

FIGURE 12. A comparison of the profiles within the quasi-steady inner region for $\Lambda = 2$ and $t = 100$. Numerical results (circles) resolving the sink with 8 grid points across (20 grid points in total) compare with both the model of constant height above the sink (dashed) and the model resolving the profile above the sink (solid). The inset shows an expanded view of the region within the sink.

REFERENCES

ACTON, J. M., HUPPERT, H. E. & WORSTER, M. G. 2001 Two-dimensional viscous gravity currents flowing over a deep porous medium. *J. Fluid Mech.* **440**, 359–380.

ANDERSON, D. M., MCLAUGHLIN, R. M. & MILLER, C. T. 2003 The averaging of gravity currents in porous media. *Phys. Fluids* **15** (10), 2810–2829.

AVCI, C. B. 1994 Evaluation of flow leakage through abandoned wells and boreholes. *Wat. Resour. Res.* **30** (9), 2565–2578.

BARENBLATT, G. I. 1996 *Scaling, Self-Similarity, and Intermediate Asymptotics*. Cambridge University Press.

BEAR, J. 1972 *Dynamics of Fluids in Porous Media*. Dover.

BICKLE, M., CHADWICK, A., HUPPERT, H. E., HALLWORTH, M. & LYLE, S. 2007 Modelling carbon dioxide accumulation at Sleipner: implications for underground carbon storage. *Earth Planet. Sci. Lett.* **255**, 164–176.

BLEANEY, B. I. & BLEANEY, B. 1976 *Electricity and Magnetism*, 3rd edn., vol. 1. Oxford University Press.

BOLSTER, D., DENTZ, M. & CARRERA, J. 2009 Effective two-phase flow in heterogeneous media under temporal pressure fluctuations. *Water Resour. Res.* **45**, W05408, doi:10.1029/2008WR007460, 1–14.

Chen, L. Y., Goldenfeld, N. & Oono, Y. 1991 Renormalization-group theory for the modified porous-medium equation. *J. Fluid Mech.* **44**, 6544–6550.

Farcas, A. & Woods, A. W. 2009 The effect of drainage on the capillary retention of CO_2 in a layered permeable rock. *J. Fluid Mech.* **618**, 349–359.

Hesse, M. A., Tchelepi, H. A., Cantwell, B. J. & Orr, F. M. Jr. 2007 Gravity currents in horizontal porous layers: transition from early to late self-similarity. *J. Fluid Mech.* **577**, 363–383.

Huppert, H. E. 2006 Gravity currents: a personal perspective. *J. Fluid Mech.* **554**, 299–322.

Huppert, H. E. & Woods, A. W. 1995 Gravity-driven flows in porous layers. *J. Fluid Mech.* **292**, 55–69.

Lake, L. 1989 *Enhanced Oil Recovery*. Prentice Hall.

Lyle, S., Huppert, H. E., Hallworth, M., Bickle, M. & Chadwick, A. 2005 Axisymmetric gravity currents in a porous medium. *J. Fluid Mech.* **543**, 293–302.

Neufeld, J. A. & Huppert, H. E. 2009 Modelling carbon dioxide sequestration in layered strata. *J. Fluid Mech.* **625**, 353–370.

Neufeld, J. A., Vella, D. & Huppert, H. E. 2009 The effect of a fissure on storage in a porous medium. *J. Fluid Mech.* **639**, 239–259.

Nordbotten, J. M. & Celia, M. A. 2006 Similarity solutions for fluid injection into confined aquifers. *J. Fluid Mech.* **561**, 307–327.

Nordbotten, J. M., Celia, M. A. & Bachu, S. 2004 Analytical solutions for leakage rates through abandoned wells. *Wat. Resour. Res.* **40** (4), W04204, doi:10.1029/2003WR00297, 1–10.

Nordbotten, J. M., Celia, M. A., Bachu, S. & Dahle, H. 2005 Semianalytical solution for CO_2 leakage through an abandoned well. *Environ. Sci. Technol.* **39**, 602–611.

Nordbotten, J. M., Kavetski, D., Celia, M. A. & Bachu, S. 2009 Model for CO_2 leakage including multiple geological layers and multiple leaky wells. *Environ. Sci. Technol.* **43**, 743–749.

Orr, F. M. Jr. 2009 Onshore geological storage of CO_2. *Science* **325**, 1656–1658.

Pacala, S. & Socolow, R. 2004 Stabilization wedges: solving the climate problem for the next 50 years with current technology. *Science* **305**, 968–972.

Phillips, O. M. 2009 *Geological Fluid Dynamics: Sub-Surface Flow and Reactions*. Cambridge University Press.

Press, W. H., Teukolsky, S. A., Vetterling, W. T. & Flannery, B. P. 1997 *Numerical Recipes in Fortran 77: The Art of Scientific Computing*, 2nd edn. Cambridge University Press.

Pritchard, D. 2007 Gravity currents over fractured substrates in a porous medium. *J. Fluid Mech.* **584**, 415–431.

Pritchard, D. & Hogg, A. J. 2002 Draining viscous gravity currents in a vertical fracture. *J. Fluid Mech.* **459**, 207–216.

Pritchard, D., Woods, A. W. & Hogg, A. J. 2001 On the slow draining of a gravity current moving through a layered permeable medium. *J. Fluid Mech.* **444**, 23–47.

Spannuth, M. J., Neufeld, J. A., Wettlaufer, J. S. & Worster, M. G. 2009 Axisymmetric viscous gravity currents flowing over a porous medium. *J. Fluid Mech.* **622**, 135–144.

Vella, D. & Huppert, H. E. 2006 Gravity currents in a porous medium at an inclined plane. *J. Fluid Mech.* **555**, 353–362.

Vella, D, Neufeld, J. A., Huppert, H. E. & Lister, J. R. 2010 Leakage from gravity currents in a porous medium. Part 2. A line sink. *J. Fluid Mech.* doi:10.1017/S002211201000491X.

Woods, A. W. & Farcas, A. 2009 Capillary entry pressure and the leakage of gravity currents through a sloping layered permeable rock. *J. Fluid Mech.* **618**, 361–379.